Weather and Climate Extremes 52 (2026) 100897

Contents lists available at ScienceDirect

Weather and Climate Extremes

journal homepage: www.elsevier.com/locate/wace

Projecting hurricane risk in Atlantic Canada under climate change

Saeed Saviz Naeini [a], Reda Snaiki [a,*], Alejandro Di Luca [b]

[a] Department of Construction Engineering, École de Technologie Supérieure, Université Du Québec, Montréal, Québec, Canada
[b] Département des Sciences de La Terre et de L'Atmosphère, Centre pour L'étude et La Simulation Du Climat à L'échelle Régionale (ESCER), Université Du Québec à Montréal, Montréal, Québec, Canada

ARTICLE INFO

Keywords:
Tropical cyclones
Wind
Coastal flooding
Climate change
Risk assessment

ABSTRACT

Atlantic Canada faces significant tropical cyclone (TC) threats from damaging winds and coastal flooding that are projected to intensify under climate change. This study adopts a two-stage framework. First, the evolution of wind and coastal-flood hazards is quantified from a historical baseline (1979–2014) to two future periods: a near future (2024–2059) and a far future (2060–2095). Hazard fields are constructed from large ensembles of physics-informed synthetic TC tracks, and changes are evaluated in return-period wind speeds and in inundation depth and extent, with sea-level rise included for flood projections. The second stage estimates TC risk using wind as an operational proxy for total loss, combining the simulated wind fields with exposure data and a vulnerability relationship to compute expected damages. This design clarifies how physical drivers change and how those shifts translate into loss potential without requiring fully coupled compound-loss modeling. Results indicate an intensification of wind extremes and a substantial amplification of coastal inundation, yielding higher wind-proxy risk for many coastal communities. Spatial patterns show a heterogeneous escalation of risk concentrated along exposed shorelines and urban corridors. This comprehensive analysis of both hazard evolution and proxy risk provides decision-ready evidence on where and by how much TC losses are likely to grow. The approach clarifies the link between physical drivers and loss potential, ensuring compatibility with standard wind-centric workflows used in engineering and insurance practice.

1. Introduction

Tropical cyclones (TCs), known as hurricanes in the Atlantic basin, rank among the planet's most destructive natural hazards, posing significant threats to coastal populations and infrastructure worldwide (Almeida et al., 2019; Mendez-Tejeda and Hernández-Ayala, 2023). Their impacts are multifaceted, driven primarily by intense winds, torrential rainfall, and storm surge which, when combined with astronomical tides and waves, can lead to devastating coastal flooding (Naeini and Snaiki, 2024; Nofal et al., 2023). A growing scientific consensus, documented in reports such as the Sixth Assessment Report of the Intergovernmental Panel on Climate Change (Seneviratne et al., 2021), confirms that anthropogenic climate change is altering TC characteristics (Balaguru et al., 2023; Kossin, 2018; Lee et al., 2023; Walsh et al., 2016). While trends in overall frequency remain uncertain, overall projections suggest an increase in the intensity and rainfall rates of the strongest storms, alongside potential poleward shifts in tracks (Seneviratne et al., 2021; Gori et al., 2022; Lin et al., 2023a; Reed et al., 2022; Snaiki and Parida, 2023; Studholme et al., 2022; Tu et al., 2022). These changes are physically linked to rising sea surface temperatures, increased atmospheric moisture content and changes in the general circulation in a warming world (Emanuel, 2005; Knutson et al., 2015; Salarieh et al., 2023).

Atlantic Canada, with its extensive coastline bordering the North Atlantic, is frequently affected by powerful storm systems, including TCs undergoing extratropical transition as they move northward (Garin et al., 2024; Jung and Lackmann, 2023; Plante et al., 2015; Zadra et al., 2014). The region's vulnerability to high winds and coastal flooding is amplified by considerable populations, critical infrastructure, and vital economic sectors concentrated in its coastal zones (Li, 2023; Pang et al., 2024; Vasseur et al., 2022). Recent history provides stark reminders of this vulnerability, with devastating impacts from storms like Hurricane Juan (2003), Igor (2010), Dorian (2019), and Fiona (2022), which caused widespread damage across the region (Aziz, 2021; Masson, 2014; Straub, 2024; Taylor et al., 2019). In response to this threat, previous studies have begun to assess the potential impacts of climate change on future TC hazards (Mendez-Tejeda and Hernández-Ayala, 2023; Balaguru et al., 2023; Cousineau and Murphy, 2022; Jiang and Perrie, 2008;

* Corresponding author.
E-mail address: reda.snaiki@etsmtl.ca (R. Snaiki).

https://doi.org/10.1016/j.wace.2026.100897
Received 31 October 2025; Received in revised form 28 March 2026; Accepted 30 March 2026
Available online 3 April 2026

Li et al., 2022; Trepanier, 2020). However, many of the prior assessments have often examined one component of the overall threat at a time, such as projecting changes in storm surge, wind speeds, or rainfall rates. Furthermore, while some recent studies have attempted to translate these changing hazards into comprehensive risk assessments, they are often limited by simplified modeling assumptions (Knutson et al., 2015; Rana et al., 2022; Ryan and Bristow, 2024) or by focusing on other geographical locations (Do and Kuleshov, 2023; Forzieri et al., 2016; Liu, 2024; Sahoo and Bhaskaran, 2018). Therefore, a dedicated analysis for Atlantic Canada that characterizes the non-stationary nature of both wind and flood hazards, while also providing a quantitative estimate of the total resulting risk, represents a key opportunity for advancing regional understanding.

Given Atlantic Canada's demonstrated vulnerability, understanding how TC hazards will evolve under climate change is a critical research priority. Projecting this evolution is complex because it depends on the interplay among changes in storm frequency and intensity across the Atlantic basin, shifts in typical storm tracks, and the dynamics of extratropical transition. Therefore, robust, forward-looking risk assessments are indispensable for clarifying these future threats and enhancing coastal resilience (Chouinard et al., 2017; Manuel et al., 2015; Provan et al., 2022; Thompson et al., 2009; Vasseur et al., 2017). A multi-hazard framing helps capture the compound nature of TCs, where high winds and coastal inundation may coincide in space and time; single-hazard analyses can overlook such interactions (Carney et al., 2022; Hillier et al., 2020; Nofal et al., 2021; Stalhandske et al., 2024; Tilloy et al., 2019; Ward et al., 2022). Consistent, forward-looking assessments therefore benefit from first quantifying changes in both wind and coastal-flood hazards and then evaluating the implications for regional loss potential. Accurately quantifying future risk further requires methodologies that integrate probabilistic hazard modeling under non-stationary climate forcing with appropriate representations of exposure and vulnerability (Nofal et al., 2021; Kameshwar and Padgett, 2014).

This study provides a quantitative assessment of evolving TC risk in Atlantic Canada through a two-stage framework. The analysis first characterizes the non-stationary nature of two primary physical hazards, namely wind and coastal flooding, from a historical baseline (1979-2014) through two future periods representing the near-future (2024-2059) and far-future (2060-2095), using projections from two GCMs. This is achieved by driving wind and coastal flooding hazard models with large ensembles of physics-based synthetic TC tracks. The study then quantifies the evolution of total TC risk by integrating the projected wind hazard, which serves as a proxy for total impact, with exposure and vulnerability data. The key aims are to quantify the magnitude and spatial distribution of these escalating threats and highlight future risk hotspots. Ultimately, this research provides a forward-looking perspective on Atlantic Canada's evolving risk profile, offering critical evidence for proactive adaptation planning.

2. Methodology

2.1. Overall framework

The methodology in this study is structured as a two-stage framework: a comprehensive hazard assessment followed by a risk calculation. The first stage characterizes two distinct physical hazards, both driven by the same ensemble of synthetic TC events (Sect. 2.2). Wind hazard is modeled through hazard footprints of maximum sustained surface winds (Sect. 2.3.1), while coastal flood hazard is characterized through inundation depth maps generated using a bathtub approach that incorporates projected sea-level rise (Sect. 2.3.2). The second stage quantifies the overall TC risk. In this stage, wind hazard is used as an operational proxy for structural damage and associated regional losses, while acknowledging that total TC impacts arise from compound hazards, including coastal flooding and heavy rainfall. The risk assessment combines the wind hazard footprints with BlackMarble-derived exposure data (Sect. 2.4; Román et al., 2018) and an adapted Emanuel-type vulnerability function (Sect. 2.5; Eberenz et al., 2021; Emanuel, 2011). This approach allows for a quantitative assessment of total risk alongside a spatial characterization of the two primary evolving hazards. A schematic overview of this workflow is presented in Fig. 1.

2.2. Synthetic tropical cyclone track generation

To generate statistically robust TC event sets that overcome the limitations of the historical record and allow for analysis under future climate scenarios, a physics-informed synthetic TC track model was employed. This approach leverages information from broader geographic regions and climate simulations to populate datasets suitable for estimating the probability of low-frequency, high-impact events. The model simulates the full lifecycle of TCs through three core modules: genesis, translation, and intensity. A schematic illustrating this track generation process is presented in Fig. 2.

The genesis module utilizes a stochastic approach, randomly seeding potential storm disturbances across space and time within the simulation domain. These initial seeds are then allowed to evolve based on their interaction with the ambient environmental conditions, mimicking observed patterns of TC formation (Emanuel, 2022). The translation module governs the storm's trajectory using the beta-and-advection framework (Emanuel et al., 2006; Lin et al., 2023b). The storm's translational velocity ($\mathbf{v}_t$) is calculated at each time step based on the influence of the large-scale environmental winds and a drift component related to the Earth's rotation ($\mathbf{v}_\beta$). The environmental winds ($\mathbf{v}_{850}$ and $\mathbf{v}_{250}$) are the daily-averaged zonal and meridional wind components at the 850-hPa and 250-hPa pressure levels, respectively. In our analysis, wind fields at the storm's location are extracted from either the ERA5 reanalysis or two CMIP6 GCM simulations. The relationship is expressed as:

$$\mathbf{v}_t = (1-\alpha)\mathbf{v}_{250} + \alpha\mathbf{v}_{850} + \mathbf{v}_\beta \cos(\phi) \tag{1}$$

where ϕ is the latitude of the storm's center and α is a steering coefficient determining the relative influence of the upper and lower-level winds. The steering coefficient is parameterized as a function of the storm's intensity (maximum wind speed), reflecting the physical principle that stronger storms are steered by a deeper atmospheric layer (Lin et al., 2023b).

For each seeded storm, the intensity module simulates the evolution of the storm's maximum azimuthal wind speed (v) based on the FAST (Fast Intensity Simulator) model framework (Emanuel, 2017). This simplified physical model uses a coupled system of equations tracking both the maximum wind speed and the inner-core moisture (m), incorporating key environmental influences. Specifically, the maximum wind speed (v) refers to the peak axisymmetric (rotational) wind at the radius of maximum winds, and the inner-core moisture (m) is a non-dimensional bulk variable representing the core's saturation. After asymmetries are added to the model's wind, the final reported value represents a 1-min sustained wind speed. The core equations are (Lin et al., 2023b):

$$\frac{dv}{dt} = \frac{1}{2}\frac{C_k}{h}\left[\alpha_o \beta V_p^2 m^3 - \left(1-\gamma m^3\right)v^2\right] \tag{2a}$$

$$\frac{dm}{dt} = \frac{1}{2}\frac{C_k}{h}\left[(1-m)v - \chi S m\right] \tag{2b}$$

where C_k is the surface enthalpy exchange coefficient, h is the boundary layer height, V_p is the potential intensity derived from the environmental thermodynamics, α_o relates to ocean interaction, S is the vertical wind shear, and other parameters (β, γ, χ) depend on environmental thermodynamic properties like entropy deficits and surface humidity (Emanuel, 2017). Environmental variables are taken from the

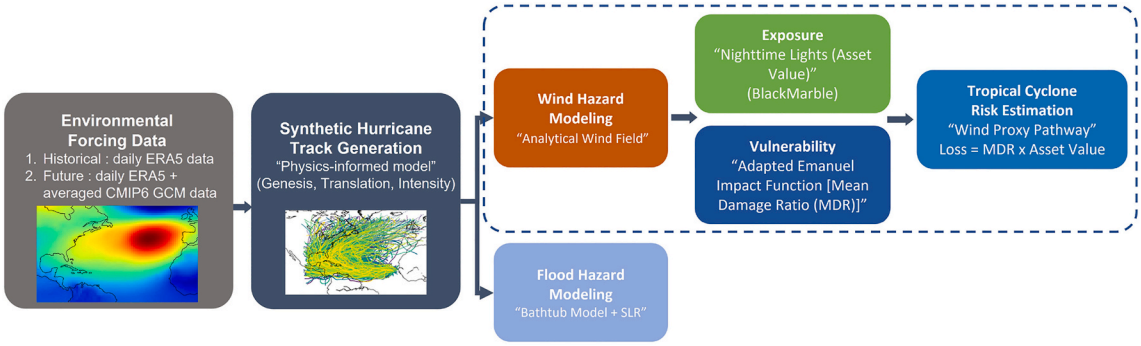

Fig. 1. Schematic overview of the proposed risk estimation methodology.

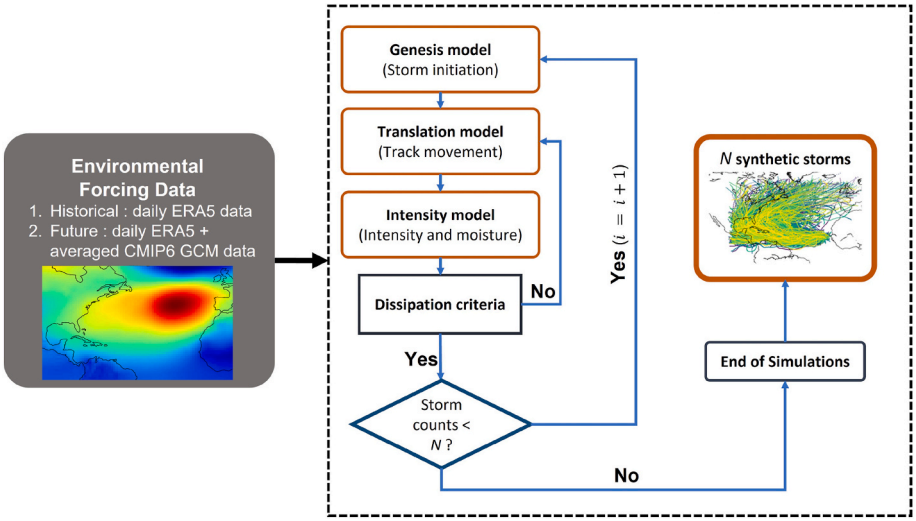

Fig. 2. Schematic of the synthetic TC track generation process.

background climate fields at the storm location with the following temporal resolutions: daily-mean winds at 850 and 250 hPa (used to compute *S*) and monthly-mean thermodynamic properties, including sea-surface temperature, air temperature, mean sea level pressure, and specific humidity.

For the historical reference period (1979-2014), the track and intensity models are forced with data from the ERA5 reanalysis. The model configuration reproduces historical TC statistics in line with validations against the IBTrACS database reported by prior studies (Lin et al., 2023b; Snaiki and Wu, 2025). To complement basin-scale validations against IBTrACS reported in prior studies, an additional regional consistency check is performed for Atlantic Canada. Modeled historical extreme winds from the downscaling framework are compared with the National Building Code of Canada (NBCC) Appendix C 50-year reference hourly wind speeds at representative sites (Halifax, Charlottetown, and St. John's), as shown in Fig. 3. The NBCC reference wind speeds are derived from long-term station observations and are standardized to 10 m height in flat open terrain and to the code's nominal 1-h averaging period; the 50-year return values are estimated from annual maxima using the Gumbel extreme-value distribution (method of moments), following the NBCC Appendix C procedure. The comparison is intentionally conducted at the 50-year level (the standard design reference in the code), because shorter return periods are typically governed by non-TC synoptic winds; benchmarking those levels using a TC-origin synthetic event set would therefore be inappropriate. This assessment is intended as a regional plausibility check of return levels and provides context for interpreting the subsequent hazard and risk analyses. As shown in Fig. 3, the simulated 50-year wind speeds exhibit close

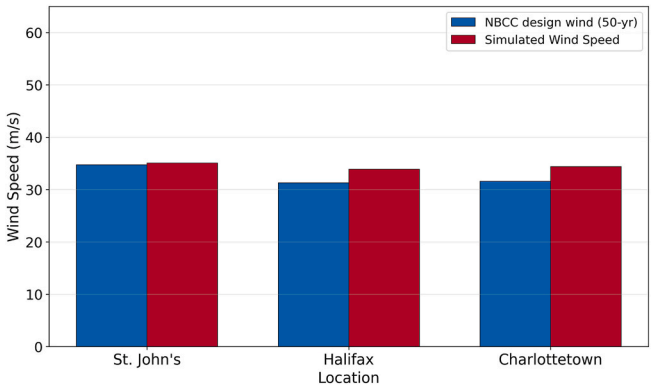

Fig. 3. Comparison of simulated and National Building Code of Canada (NBCC) Appendix C reference 50-year return-period nominal 1-h mean wind speeds (10 m, open terrain) at selected Atlantic Canada sites.

agreement with NBCC reference values across all three sites; modest positive deviations are observed for Halifax and Charlottetown, while St. John's aligns particularly well.

To generate simulations for future climates, a delta-change approach was employed as a bias correction method to reduce the impact of systematic errors often found in raw GCM outputs. First, climate change perturbations ('deltas') for key environmental fields were calculated using two CMIP6 GCMs (EC-Earth3P-HR and CMCC-CM2-SR5 under the SSP5-8.5 scenario) for the mid-century (2024–2059) and late-century

(2060–2095) periods. Thermodynamic fields (e.g., sea surface temperature, air temperature) use monthly-mean deltas (future monthly climatology minus historical monthly climatology), which are added to the corresponding ERA5 fields. Future environmental wind fields ($\mathbf{v}_{850}$ and $\mathbf{v}_{250}$) are obtained by superimposing calendar-day climatological deltas (future daily climatology minus historical daily climatology) onto the corresponding ERA5 wind fields. The $\mathbf{v}_{850}$ and $\mathbf{v}_{250}$ fields are evaluated at the storm-center location at each time step using bilinear interpolation of the gridded winds (i.e., storm centers are treated as continuous coordinates rather than being constrained to grid points). The resulting 'perturbed' ERA5 fields serve as the forcing data for the future simulations. The main advantage of this method is that it preserves the realistic and detailed weather patterns of the ERA5 baseline, while using the GCMs only to provide the projected climate change signal. This ensures that the TC simulations are not overly influenced by underlying GCM biases (Hall et al., 2024; Knutson et al., 2008; Prein et al., 2017; Rasmussen et al., 2011; Schär et al., 1996; Willison et al., 2015). This method, often referred to as the pseudo-global warming (PGW) approach, was first introduced by Schär et al. (1996) and has since been widely used to study future changes in tropical and extratropical cyclones (Knutson et al., 2008; Willison et al., 2015), snowfall over complex terrain (Rasmussen et al., 2011), thunderstorms across North America (Prein et al., 2017) and extreme temperature and precipitation (Hall et al., 2024). Using this framework, 10,000 years of synthetic TC activity were simulated for each climate period to ensure a statistically robust event set for the subsequent analyses. The output for each synthetic TC is an hourly time series detailing its geographical position (latitude, longitude), minimum sea level pressure (MSLP), maximum sustained wind speed (V_{max}), and radius of maximum wind (R_{max}).

2.3. Hazard modeling

Following the generation of synthetic TC tracks (Sect. 2.2), the next step is to model the physical hazards associated with each storm event. This process involves two parallel streams: one for wind and one for coastal flooding. First, an analytical wind field model is used to generate a spatial "footprint" of the maximum sustained surface wind speeds for each synthetic TC (detailed in Sect. 2.3.1). Second, a bathtub model is employed to simulate the corresponding coastal flood footprint, estimating the maximum inundation depth (detailed in Sect. 2.3.2). This procedure results in a large ensemble of event-based hazard footprints. This ensemble is then statistically analyzed to produce probabilistic hazard maps, which show hazard intensities (e.g., wind speed or flood depth) for various return periods (detailed in Sect. 2.3.3).

2.3.1. Wind hazard modeling

The simulation of the TC surface wind field for each synthetic event involved several steps. First, the tangential component of the gradient wind ($v_{\theta g}$) was calculated analytically. This component represents the wind speed in the free atmosphere above the boundary layer, balancing pressure gradient, Coriolis, and inertial forces associated with the moving storm. The gradient wind component at a given radius (r) and azimuth (θ) is calculated as (Holland, 1980; Snaiki and Wu, 2017):

$$v_{\theta g} = \frac{1}{2}\left(- c \cdot sin(\theta - \theta_0) - fr\right) + \left[\left(\frac{-c \cdot sin(\theta - \theta_0) - f \cdot r}{2}\right)^2 + \frac{r}{\rho}\frac{\partial P}{\partial r}\right]^{\frac{1}{2}} \quad (3)$$

where c is the storm's translational speed and θ_0 is its direction of motion (obtained from the synthetic track, Sect. 2.2), f is the Coriolis parameter (dependent on latitude ϕ), ρ is the air density, and $\frac{\partial P}{\partial r}$ is the radial pressure gradient. The pressure gradient term was derived by differentiating the Holland pressure profile model (Holland, 1980), which is defined using storm parameters (MSLP, R_{max}, Holland B parameter) from the synthetic track model. The radial component of the gradient wind (v_{rg}) was considered negligible, consistent with previous studies (Meng et al., 1995). The magnitude of the gradient wind is thus $V_g \approx |v_{\theta g}|$.

Second, the calculated gradient wind speed (V_g) was reduced to estimate the standard 10-m, 1-min sustained surface wind speed (V_s) using empirical conversion factors. This step accounts for the frictional effects within the planetary boundary layer, following methodologies used in TC risk assessment studies (e.g. Lin and Chavas, 2012). Specifically, a spatially varying factor based on underlying land cover derived from the World Meteorological Organization (WMO) dataset was used (Harper et al., 2010). For this analysis, the land cover is assumed to remain constant across all historical and future time periods. To efficiently generate the wind hazard information, the analysis focused on the impact of storms passing near each location of interest. For each point on a predefined grid, synthetic storm tracks passing within a 250 km radius were identified as potentially influential. For each relevant track segment, the maximum asymmetric surface wind speed at that specific grid point was determined. This location-specific maximum wind speed serves as the primary input for constructing event-based hazard footprints and for the probabilistic hazard assessment described in Sect. 2.3.3.

2.3.2. Coastal flood hazard modeling

The coastal flood hazard associated with each synthetic TC was assessed using a bathtub modeling approach (e.g. Didier et al., 2019; Poulter and Halpin, 2008; Shepard et al., 2012), a simplified method that identifies potentially inundated areas by comparing the estimated peak coastal water level during an event against land surface elevation data. The estimation of the peak water level (η_{peak}) is central to this approach and was determined by summing two key components: the storm surge generated by the TC and the projected Sea Level Rise (SLR). Specifically, the storm surge height, η_{surge}, was estimated using the empirical wind–surge relationship of (Xu, 2010) expressed as $\eta_{surge} = 0.1023\, max(V_{max} - 26.8224, 0) + 1.8288$, where V_{max} denotes the event maximum coastal surface wind speed. This formulation provides a computationally efficient transfer function between coastal wind speed and open-coast surge height, calibrated from National Weather Service SLOSH 'MEO' (Maximum Envelope of Water) pre-run outputs via linear interpolation. As reported in (Xu, 2010), the relationship reproduces SLOSH-based surge estimates for benchmark TCs (e.g., Hugo, 1989; Andrew, 1992) with typical errors on the order of ±20% relative to observed surge. For each synthetic event, V_{max} was first computed along the coastline and then converted to η_{surge} using the above expression. The peak coastal water level was subsequently obtained as $\eta_{peak} = \eta_{surge} + \eta_{SLR}$, where η_{SLR} is the period-specific sea-level-rise increment (2024–2059 or 2060–2095). While relative SLR projections for Atlantic Canada exhibit some spatial variability (Lee et al., 2023), regionally-averaged values were adopted to represent the overall increase in baseline water levels for this screening-level inundation assessment. For each time slice, central (median) SLR estimates were used rather than upper-tail (e.g., 95th-percentile) projections. Based on high-emission scenario (SSP5-8.5) projections, an SLR of approximately 0.5 m was used for the near-future period (2024–2059), and 1 m was used for the far-future period (2060–2095) (Lee et al., 2023). The final peak water level was thus calculated as $\eta_{peak} = Storm\ surge + SLR$. The influence of astronomical tides was not explicitly included in this calculation, representing a focus on the storm-induced and climate-change-driven water level components.

The subsequent inundation mapping involved applying the calculated η_{peak} for each event to a high-resolution Digital Elevation Model (DEM) representing the coastal topography of the study area. All land grid cells hydraulically connected to the coast and having an elevation lower than the estimated η_{peak} are identified as inundated. The inundation depth at each affected grid cell was then computed as $Depth = \eta_{peak} - Ground\ Elevation$. This mapping was performed at a spatial res-

olution suitable for analysis with the building inventory data.

It is important to acknowledge the inherent assumptions associated with the bathtub model employed in this study. The approach assumes hydrostatic equilibrium (water instantly fills connected areas to the peak level) and neglects hydrodynamic effects such as flow momentum, friction, or the temporal evolution of the inundation. Furthermore, the contributions of wave setup and runup are neglected. The model also treats the landscape as static and does not account for morphological changes during the storm or the presence and potential failure of local flood defense structures unless these features are accurately resolved within the underlying DEM. Given these simplifications, the coastal-flood component is used here primarily to support a consistent, screening-level comparison of spatial inundation susceptibility and its projected changes between time periods, rather than to predict event-specific flood depths for design applications. Inundation is computed relative to mean sea level (MSL) (i.e., a fixed tidal-stage reference), and astronomical tides are not included; therefore, mapped flood depths should be interpreted as conditional-on-MSL and as a conservative lower bound relative to high-tide conditions. Coastal flooding in Atlantic Canada can be compound, with contributions from tides, wind waves (setup/runup), pluvial runoff, and fluvial discharge that vary by coastline and storm characteristics; these processes are not represented in the present module, which is limited to storm surge plus relative sea-level rise. The resulting inundation maps should therefore be interpreted as first-order indicators of potential flooding and of how changes in surge forcing and baseline sea level may shift inundation susceptibility over time under a fixed set of assumptions.

The output of this coastal flood hazard modeling stage consists of a set of flood depth footprints, one for each synthetic TC event, illustrating the maximum estimated inundation depth across the affected coastal regions within the study area.

2.3.3. Probabilistic hazard assessment

From the 10,000 years of simulated TC activity, the large ensembles of hazard footprints for both wind (Sect. 2.3.1) and coastal flooding (Sect. 2.3.2) were statistically aggregated to derive probabilistic hazard estimates. This process translates the collection of individual storm impacts into measures of hazard intensity (e.g., wind speed or flood depth) that correspond to specific likelihoods or return periods. For each grid location within the study area and for each hazard type (wind and flood), a time series of the annual maximum intensity experienced over the $n = 10,000$ year simulation period was compiled. These annual maxima were then ranked in descending order, with rank $i = 1$ assigned to the highest intensity, $i = 2$ to the second highest, and so on, up to $i = n$. The annual exceedance probability (P_e) for each ranked intensity value was estimated using the empirical Weibull plotting position formula (Makkonen, 2006; Weibull, 1939):

$$P_e = \frac{i}{n+1} \tag{4}$$

The corresponding return period (RP), representing the average time interval between years experiencing an intensity of that magnitude or greater, was calculated as the inverse of the annual exceedance probability:

$$RP = \frac{1}{P_e} = \frac{n+1}{i} \tag{5}$$

Using these relationships, hazard intensity values corresponding to standard return periods of interest (e.g., 50, 100, 300, and 700 years) were determined for each grid location, typically through interpolation between the ranked values. This procedure was applied separately for wind speed and flood depth, and repeated for each climate scenario (historical: 1979-2014; near future: 2024-2059; far future: 2060-2095), allowing for comparison across time periods and scenarios.

The final outputs of the probabilistic hazard assessment stage are spatially explicit maps illustrating the estimated wind speed and flood depth associated with specific return periods (e.g., the 100-year wind speed map and the 100-year flood depth map) for each climate scenario. Hazard curves, plotting intensity against return period or annual exceedance probability for selected locations, can also be generated from this analysis.

2.4. Exposure data processing

To quantify the potential impacts from TCs, an exposure dataset was processed using BlackMarble data (Román et al., 2018). BlackMarble provides high-resolution estimates of anthropogenic nighttime light intensity, which in this study were used as a spatial proxy for population distribution. The estimated population in each grid cell, P_i, was converted to an economic exposure proxy by scaling with provincial GDP per capita for 2020, such that $E_i = P_i \times GDP_{pc_{prov,2020}}$ yielding gridded exposure values in 2020 Canadian dollars (CAD). Here, GDP per capita serves as a pragmatic proxy to translate population (inferred from nightlights) into an economic exposure measure in the absence of a detailed asset inventory. The resulting exposure grid was then resampled/formatted to match the spatial resolution of the wind-hazard footprints (Aznar-Siguan and Bresch, 2019).

2.5. Vulnerability specification

The vulnerability function translates the hazard intensity into a potential damage ratio, forming the critical link between the physical event and its economic impact. For the risk assessment in this study, where wind speed serves as the proxy for total TC impact, an adapted vulnerability function based on the work of Emanuel was employed (Eberenz et al., 2021; Emanuel, 2011). This function relates the maximum sustained surface wind speed at a given location (output from Section 2.3.1) to an expected damage ratio. BlackMarble exposure values were used to scale the vulnerability outputs, providing a consistent measure of potential impacts across affected assets. The specific functional form used in this study is illustrated in Fig. 4. The Mean Damage Degree (MDD) denotes the average fraction of damage sustained by assets conditional on being affected at a given wind intensity. The Percentage of Affected Assets (PAA) represents the fraction of exposed assets that experience any damage at that intensity. Their product, the Mean Damage Ratio (MDR = MDD × PAA), provides the expected fractional loss and forms the quantity used to compute impacts (Aznar-Siguan and Bresch, 2019).

2.6. Risk assessment

The final methodological step is a probabilistic risk assessment to

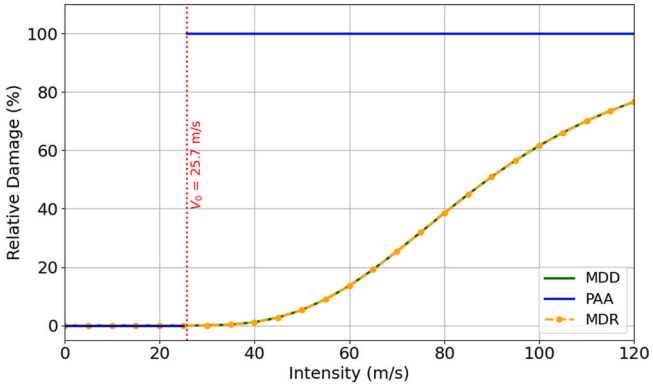

Fig. 4. Wind-to-damage vulnerability curves showing Mean Damage Degree (MDD), Percentage of Affected Assets (PAA), and Mean Damage Ratio (MDR = MDD × PAA; plotted as "Relative Damage") versus maximum sustained surface wind speed, with damage onset at $V_0 = 25.7\ m/s$ (MDR = 0 for $V < V_0$).

quantify potential economic impacts. The process begins by compiling a full damage history for each individual grid cell. Specifically, exposure and vulnerability are combined using a multiplicative loss formulation at the grid-cell level. Each grid cell is assigned an exposure value $E(x)$ (2020 CAD) derived from BlackMarble-based population proxies scaled by provincial GDP per capita (Section 2.4). For each synthetic event affecting that grid cell, the modeled maximum sustained wind speed $V(x)$ is converted to a mean damage ratio $MDR(V)$ using the wind vulnerability curves (Section 2.5), with $MDR = MDD \times PAA$. The event loss at location x is then $L_e(x) = MDR(V_e(x))E(x)$. Repeating this calculation over the full synthetic catalog yields a loss history at each grid cell. Using the catalog's event frequency (annual occurrence rates), a loss exceedance curve is constructed, from which T-year loss metrics are extracted (annual exceedance probability $= 1/T$) to generate spatial risk maps and return-period plots. (Aznar-Siguan and Bresch, 2019).

3. Case study

The hazard and risk assessment methodology detailed in Sect. 2 is applied to a case study of Atlantic Canada's coastal regions. This section first outlines the geographic scope and describes the various datasets used for the analysis (Section 3.1). Subsequently, it presents the key findings derived from the simulations (Sect. 3.2), including the characteristics of synthetic TC climatology, the projected wind and coastal flood hazards, and the resulting TC risk estimates, which are derived using the wind proxy. These results are presented across the different climate scenarios and time periods to illustrate how the hazard probabilities and risk are expected to evolve.

3.1. Study area and data

3.1.1. Study area description

The study focuses on the coastal regions of Atlantic Canada, a broad area encompassing the provinces of Nova Scotia, New Brunswick, Prince Edward Island, Newfoundland and Labrador, and the Magdalen Islands in Quebec. These regions possess an extensive and complex coastline exposed to weather systems originating in the North Atlantic, including tropical cyclones that often transition into powerful post-tropical storms (Hart and Evans, 2001). Significant portions of the population, critical infrastructure, and economic activities are concentrated in these coastal zones, making them inherently vulnerable to TC impacts such as high winds and coastal flooding (Vasseur et al., 2017; Buttle et al., 2016; Lin et al., 2019).

Fig. 5 illustrates the geographical extent of the study area where the hazard and risk simulations were conducted. For more detailed analysis, five representative locations were selected from within these regions: Halifax, Nova Scotia (44.60°, −63.47°); St. John's, Newfoundland and Labrador (47.55°, −52.71°); Saint John, New Brunswick (45.26°, −66.04°); Charlottetown, Prince Edward Island (46.22°, −63.14°); and Magdalen Islands, Quebec (47.41°, −61.90°).

3.1.2. Data sources

A variety of datasets were employed to drive the synthetic track generation, hazard modeling, exposure representation, and vulnerability assessments detailed in the methodology. The synthetic track model (Sect. 2.2) was driven by environmental conditions from the ERA5 reanalysis database for the historical period (1979-2014) (Hersbach et al., 2020). For future periods (2024-2059 and 2060-2095), corresponding variables were extracted from two GCMs from the CMIP6 project (i.e., EC-Earth3P-HR and CMCC-CM2-SR5) under the SSP5-8.5 high-emission scenario. As mentioned earlier, environmental variables are taken at different temporal resolutions, including daily-averaged zonal and meridional wind components at the 850-hPa and 250-hPa pressure levels, and monthly-mean thermodynamic properties including the sea-surface temperature (sst), air temperature, specific humidity, and mean sea level pressure. Sea level rise projections, incorporated into the flood hazard modeling (Sect. 2.3.2), were adapted from Canadian relative sea-level projections based on the IPCC Sixth Assessment Report under high-emission SSP5-8.5 scenario (Lee et al., 2023). Moreover, topographic data essential for the bathtub flood modeling (Sect. 2.3.2) were obtained from the High-Resolution Digital Elevation Model (HRDEM) database of Natural Resources Canada, providing data at 1 m × 1 m spatial resolution, referenced to the Canadian Geodetic Vertical Datum of 2013 (CGVD2013) (Canada, 2019).

The economic exposure for the risk assessment was derived from the 2020 NASA BlackMarble dataset, which provides a proxy for population

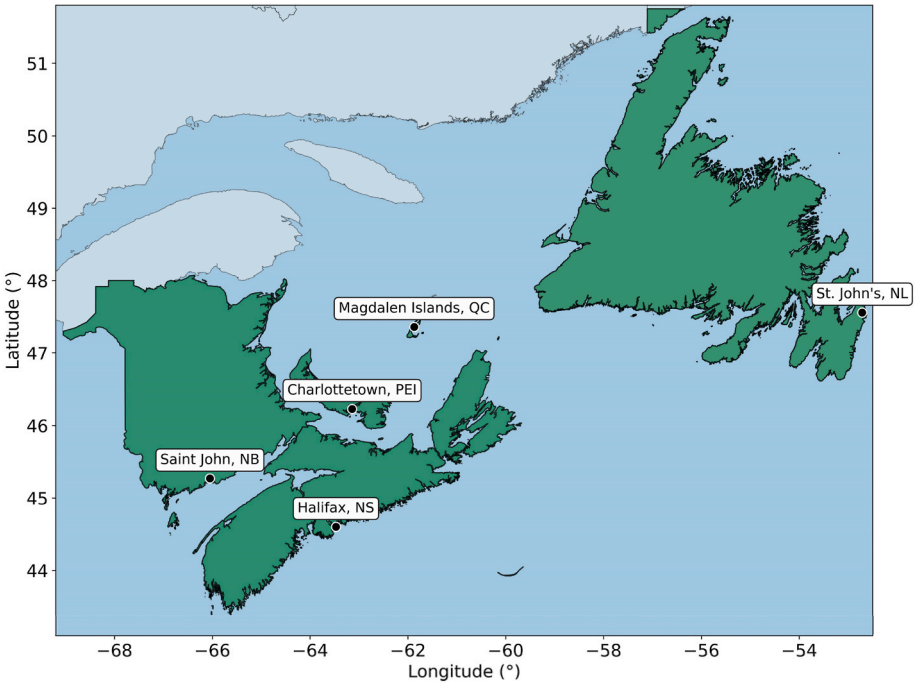

Fig. 5. Map of the Atlantic Canada study area showing the selected representative locations.

distribution at a 1 km resolution. These population estimates were then converted to an economic exposure value (in 2020 CAD) using provincial GDP per capita data from the World Bank. The vulnerability function, used to translate the wind hazard proxy into a total damage ratio, was adapted from established literature (Eberenz et al., 2021). Other parameters for the hazard models, such as surface wind reduction factors, were also retrieved from published sources (Harper et al., 2010; Xu, 2010).

3.2. Results

3.2.1. Synthetic tropical cyclone climatology

The analysis begins with an examination of the synthetic TC datasets generated for the historical (1979-2014), near-future (2024–2059), and far-future (2060–2095) periods. Each period is represented by a 10,000-year catalog containing on the order of 10^5 storms ($\sim 1.2\times10^5$), providing a large sample for estimating extreme statistics. The validity of the underlying track generation model is supported by previous validation studies against historical TC observations (e.g. Lin et al., 2023b; Emanuel, 2017; Snaiki and Wu, 2025).

To quantify changes in regional TC activity, storm frequency is defined as the number of storms passing within a 250-km radius of each location (i.e., encounter frequency), and percentage changes are calculated for future periods relative to the historical baseline. These encounter-frequency estimates are computed at five representative locations and may not capture the full spatial variability across Atlantic Canada; areas with different track geometries or coastal exposure may exhibit departures from the site-level trends reported here. The results, illustrated in Fig. 6, reveal a consistent and notable decrease in storm frequency across all selected locations and under both GCM scenarios. The magnitude of this decrease varies by location and climate model. Projections driven by the EC-Earth3P-HR model show frequency reductions generally ranging from 11% to 18%. The decreases are more pronounced under the CMCC-CM2-SR5 model, with projected declines typically between 18% and 27%. For example, under the CMCC-CM2-SR5 model, the storm frequency at Halifax is projected to decline by 22% in the near future and 25% in the far future. At St. John's, the projected decreases are even larger, at 22% for the near future and 27% for the far future. The specific percentage changes for all locations are detailed in Fig. 6, where confidence intervals are generally narrow, indicating that sampling uncertainty associated with the finite synthetic catalogue is small relative to the projected frequency changes. The confidence intervals are derived under an approximate Poisson encounter-count model, which assumes that individual storm encounters are mutually independent. Overall, these results highlight the non-stationary nature of future TC activity, with consistent declines projected across both climate models. The differences in the magnitude of decreases between the two GCMs also emphasize the substantial uncertainty inherent in GCM-driven climate impact assessments.

3.2.2. Hazard analysis

3.2.2.1. Wind hazard. Based on the synthetic TC climatology, probabilistic hazard levels were computed across Atlantic Canada. Fig. 7 presents maps illustrating the spatial distribution of the 10-m maximum sustained surface wind speeds for selected return periods (50, 100, 300, and 700 years) using the EC-Earth3P-HR model. A visual analysis reveals a clear and consistent increase in wind hazard for all return periods when progressing from the historical to the near-future and far-future scenarios. This intensification is most pronounced in the far-future period (2060-2095), with the coastal regions of Nova Scotia consistently experiencing the highest wind speeds compared to other parts of Atlantic Canada across all time periods.

To quantify the magnitude of these changes, the percentage change in the 100-year wind speed was calculated for both future periods relative to the historical baseline, as depicted in Fig. 8. The projections from the EC-Earth3P-HR model are particularly pronounced, indicating that wind speeds for the 100-year event could increase by up to 26% in the far-future scenario, with the most significant changes concentrated along the coast of Newfoundland, New Brunswick and Nova Scotia. In contrast, the CMCC-CM2-SR5 model produces a more spatially diverse pattern, with both increases and decreases in wind speeds across the region. This pattern includes reductions of up to −7% in parts of Nova Scotia, alongside localized increases reaching as high as 22% in New Brunswick.

The trend of intensifying wind hazard is further detailed in the return period plots (Fig. 9) for the five representative locations described in Section 3.1.1. A comparison of the GCM projections at these sites reveals a significant divergence. At the Nova Scotia location, the 100-year wind speed is projected to change by +4% in the near future and +9% in the far future under the EC-Earth3P-HR model. In contrast, the CMCC-CM2-SR5 model projects changes of −6% and −4% for the same periods. In the Magdalen Islands, the 300-year wind speed under EC-Earth3P-HR increases by +9% (near future) and +15% (far future), while the CMCC-CM2-SR5 model shows changes of −2% and +3%. For the Newfoundland site in the far-future, the 300-year wind speed increases by +20% with EC-Earth3P-HR, compared to a +5% increase with CMCC-CM2-SR5. Notably, the EC-Earth3P-HR model consistently

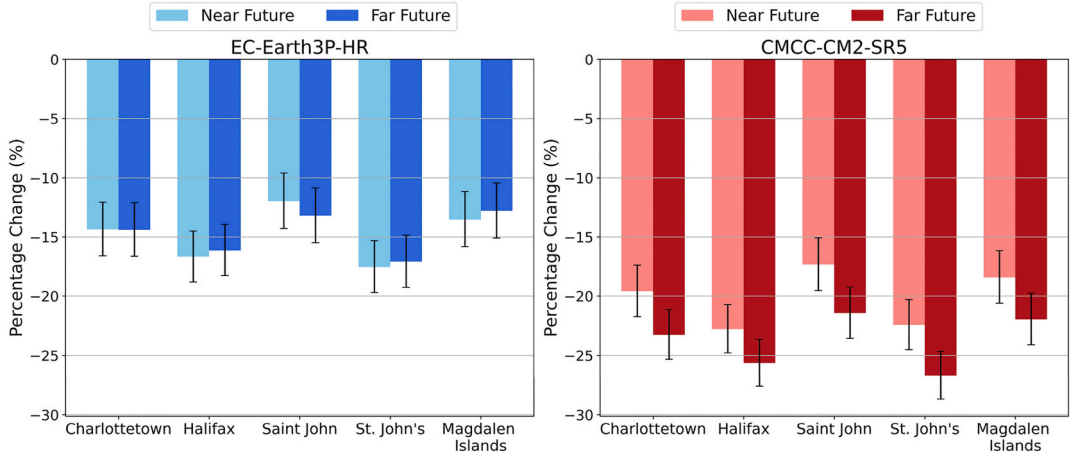

Fig. 6. Projected change in storm frequency relative (in %) to the historical period at selected locations for near and far future climate scenarios. Results are shown for two CMIP6 GCMs: EC-Earth3P-HR (left) and CMCC-CM2-SR5 (right). Error bars denote 95% confidence intervals estimated under an approximate Poisson encounter-count model (storms within 250 km over 10,000-year catalogs).

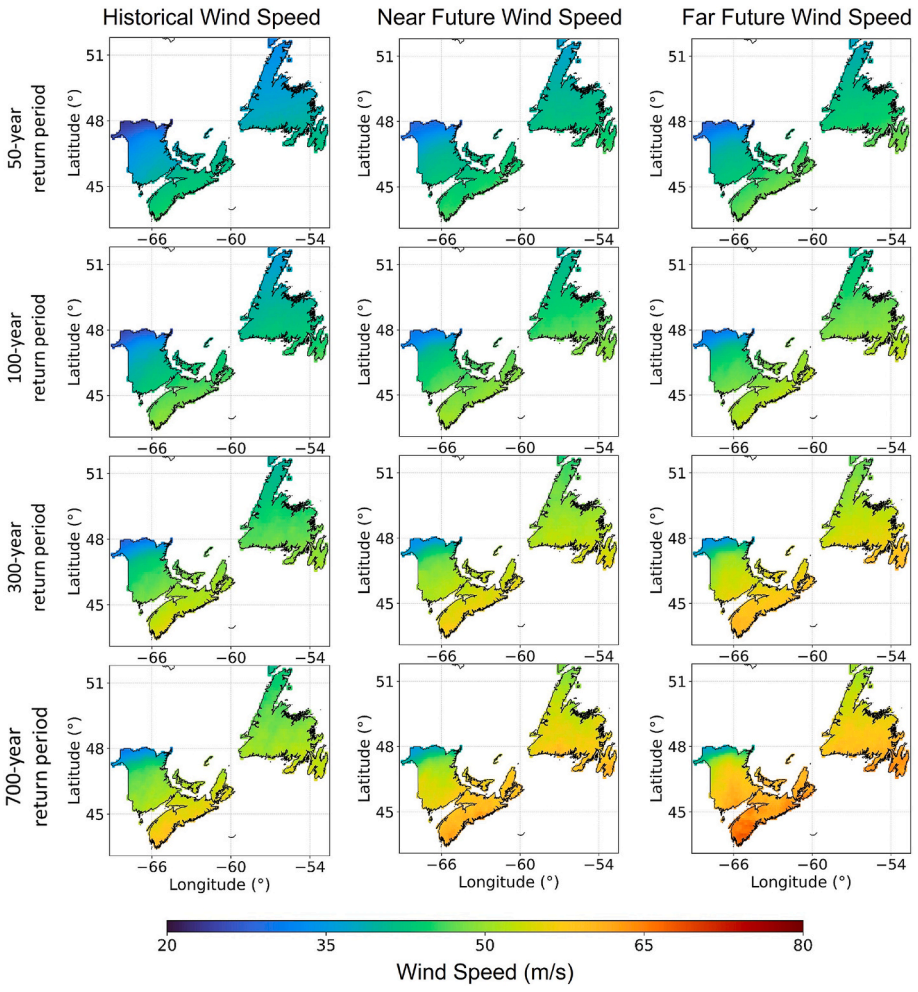

Fig. 7. Return period wind speeds across Atlantic Canada for historical and future climate scenarios using the EC-Earth3P-HR model.

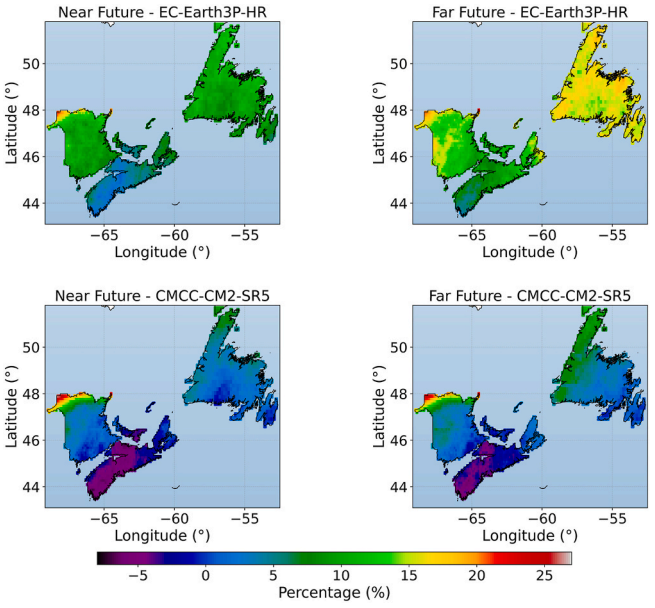

Fig. 8. Projected percentage change in 100-year wind speed for future scenarios relative to the historical baseline.

projects increases in wind speeds across return periods and locations, whereas the CMCC-CM2-SR5 model shows a more mixed response. This contrast highlights the importance of considering model uncertainty in future risk evaluations.

3.2.2.2. Flood hazard. Probabilistic hazard levels for maximum flood depth were also computed. While the broader study area encompasses all of Atlantic Canada, five representative coastal locations were selected for a detailed, high-resolution analysis to illustrate localized impacts. These sites—located within New Brunswick, Nova Scotia, Prince Edward Island, Newfoundland and Labrador, and Quebec—were modeled at a spatial resolution of approximately 30 by 55 m. To clearly illustrate the core findings, the flood hazard results presented in this section are driven by the EC-Earth3P-HR model. This focus is used for clarity, as the fundamental trends are dominated by Sea Level Rise and thus are consistent across both GCM scenarios. Fig. 10 illustrates the spatial distribution of the 100-year flood depths for three of these areas (Charlottetown, St. John's, and the Magdalen Islands). The maps clearly demonstrate the significant amplifying effect of SLR, which results in a substantial expansion of the inundated area and a notable increase in flood depths compared to scenarios without it.

The changes across all return periods are detailed in Fig. 11, which separates the impact of changing storm characteristics from the combined effect including SLR. The analysis shows that SLR is the dominant factor amplifying future flood hazard. For instance, based on projections from the EC-Earth3P-HR model, at the Halifax site, the 100-year flood depth in the far future is projected to increase by 11% due to storm changes alone; with SLR included, this increase is more than quadrupled

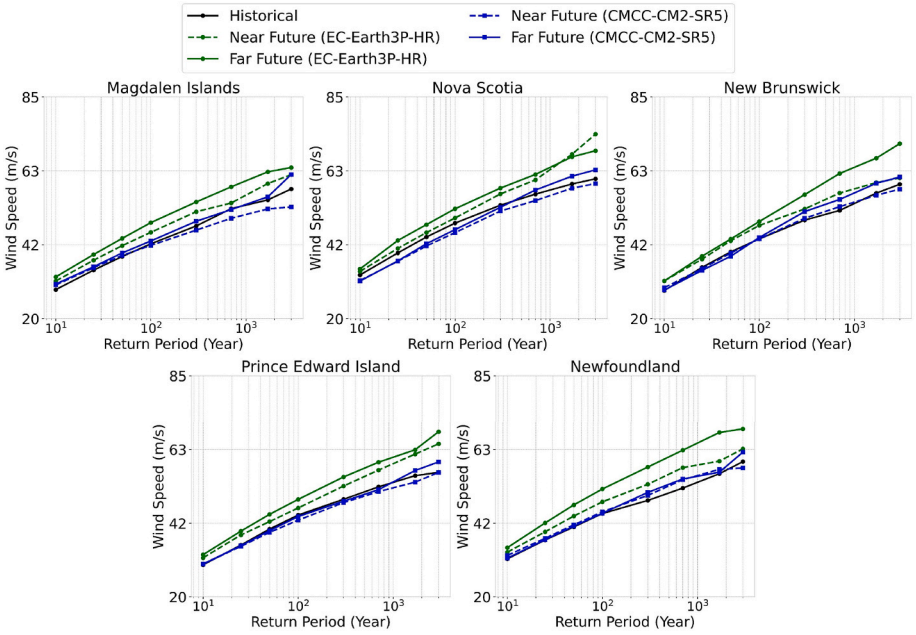

Fig. 9. Comparison of historical and projected wind speed return periods at selected locations.

to 48%. A similar amplification is seen in the Magdalen Islands, where the 300-year flood depth in the far future increases by 43% from storms alone but jumps to 102% when SLR is added. This pattern of SLR acting as the primary driver is consistent across the other analyzed locations and is also evident in projections from the CMCC-CM2-SR5 model (not shown in Fig. 11 for brevity). For example, under the CMCC-CM2-SR5 model at the Charlottetown site, the 100-year flood depth in the far future is projected to increase by 4% from storm changes alone. With the inclusion of SLR, this increase is quadrupled to 60%. These results confirm that all locations analyzed face a significant and accelerating increase in future coastal flood hazard, driven primarily by SLR. These flood-depth maps are intended as screening-level indicators under a consistent modeling framework. Detailed site-specific assessments, particularly in compound-flood settings influenced by river discharge/backwater effects and/or wave-driven processes, would require coupled hydrodynamic, wave, and hydrologic modeling with local calibration.

3.2.3. *Risk analysis*

The final step of the analysis quantifies the total economic risk from TCs. This is achieved by integrating the probabilistic wind hazard, which serves as a proxy for total TC impact, with the exposure and vulnerability models. The primary risk metric is Expected Damage (*ED*), which represents the potential loss for events of a given return period. The spatial distribution of *ED* for a 100-year return period event is illustrated in Fig. 12. The maps show a clear upward trend in risk when comparing the historical scenario to the mid- and late-century periods. The results highlight that the coastal regions of Nova Scotia and Newfoundland are projected to experience the highest absolute damages. This concentration of risk is due to a combination of significant hazard levels and a high concentration of exposed assets in those areas.

Fig. 13 provides a more detailed quantification of the increasing risk trends across various return periods for five selected regions. The aggregated damages shown in these plots were calculated by summing the *ED* values for the specific high-exposure sub-areas within each province (as depicted in Fig. 12 maps). While these aggregated damages generally increase compared to the historical baseline, the plots reveal a notable divergence between the projections from the two GCMs, highlighting significant model uncertainty. For a 300-year event in Prince Edward Island, the far-future scenario shows a 77% increase in *ED* under EC-Earth3P-HR, while the CMCC-CM2-SR5 model projects a 2% decrease. In the Magdalen Islands, damages for the same rare event rise by approximately 102% with EC-Earth3P-HR but by only 23% with CMCC-CM2-SR5. In Nova Scotia, near-future damages rise by 25% under EC-Earth3P-HR but fall by 13% under CMCC-CM2-SR5. These examples show that the EC-Earth3P-HR model consistently produces higher damage projections, whereas the CMCC-CM2-SR5 model produces both increases and decreases depending on the region.

4. Discussion

This section elaborates on the significance of the results presented in Sect. 3, interpreting the projected changes in TC climatology, the associated wind and coastal flood hazards, and the resulting total TC risk. It also addresses the implications of the non-stationary nature of these changes, discusses the methodological strengths and limitations, considers the implications for adaptation planning, and suggests directions for future research.

4.1. *Interpretation of findings*

The results of this study indicate a marked shift in the TC environment affecting Atlantic Canada over the 21st century, with implications for both wind-related impacts and coastal flooding. Projected changes are spatially heterogeneous and differ across the two GCM-driven perturbations. In the EC-Earth3P-HR-driven scenarios, wind hazard increases are generally widespread, whereas CMCC-CM2-SR5 produces a more mixed spatial response with localized increases and decreases. Overall, wind hazard tends to intensify along large portions of the Atlantic Canada coastline, while coastal flood hazard increases most strongly in low-lying areas, primarily due to rising baseline sea level. Importantly, the reported TC risk metrics reflect wind-related proxy losses only. Coastal flooding is assessed here at the hazard level and is not coupled with exposure or vulnerability to estimate flood losses; accordingly, the coastal flood component should be interpreted as a screening-level indicator of relative (directional) changes in inundation potential under consistent assumptions (including MSL reference and no tides) rather than a design-grade estimate.

A key finding is that changes in future hazard are governed less by encounter frequency than by storm intensity. Although storm frequency decreases in the synthetic catalogs at the selected locations, this

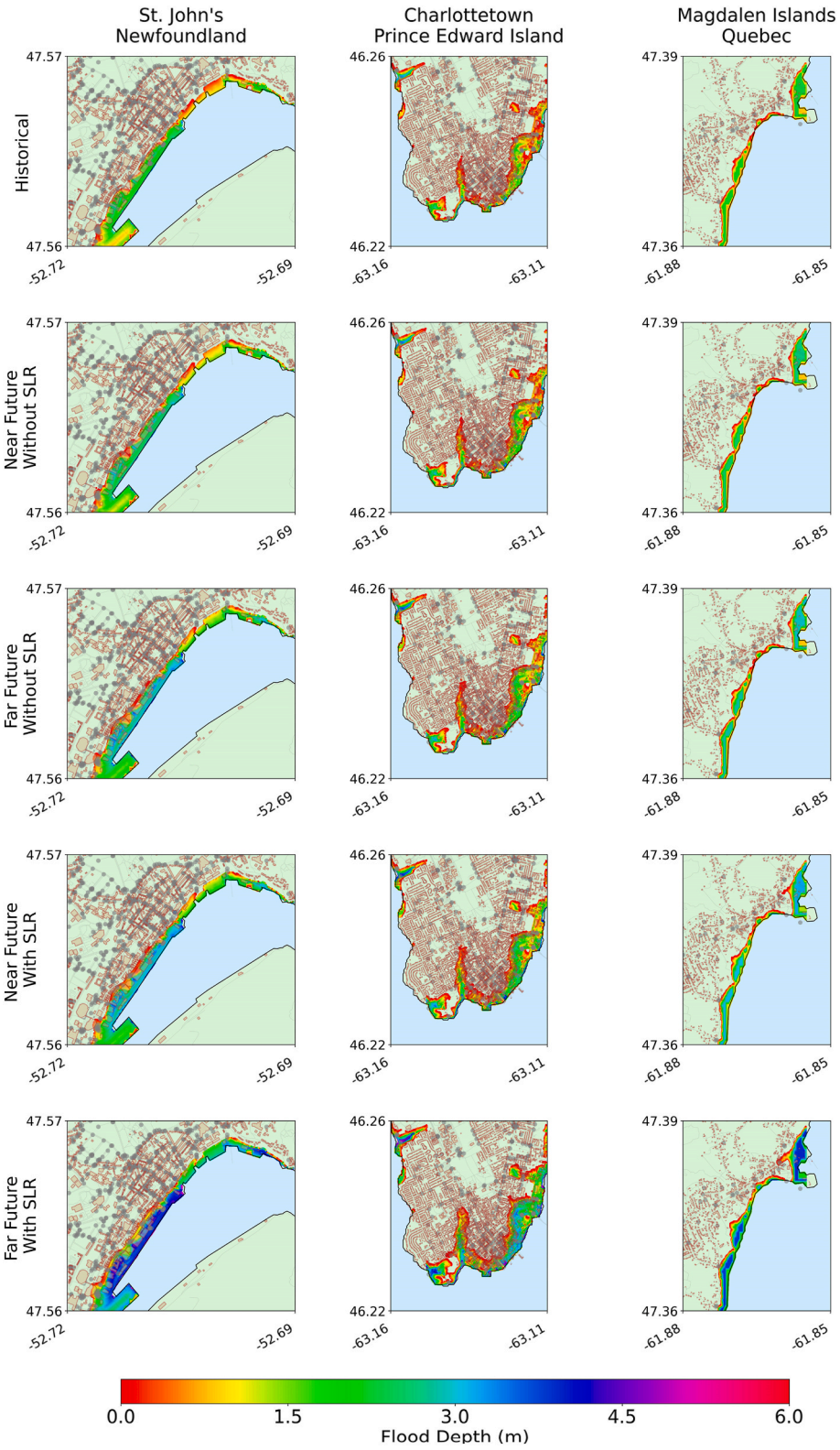

Fig. 10. Spatial distribution of 100-year coastal flooding for selected locations under historical and EC-Earth3P-HR future scenarios.

reduction is offset by increases in wind intensity across return periods, which amplifies wind-proxy losses through the vulnerability relationship. Consistent with this, the upper tail of the wind distribution strengthens in several locations and scenarios, implying that extreme winds can increase even when the total number of encounters declines. This qualitative behavior aligns with broader assessments in the literature, which indicate that total tropical cyclone frequency may decrease or remain near-constant under warming, while the fraction of the most intense storms can increase; consequently, regional risk assessments must consider intensity changes alongside encounter frequency.

Spatially, the analysis exhibits two distinct hazard signatures: (i) a

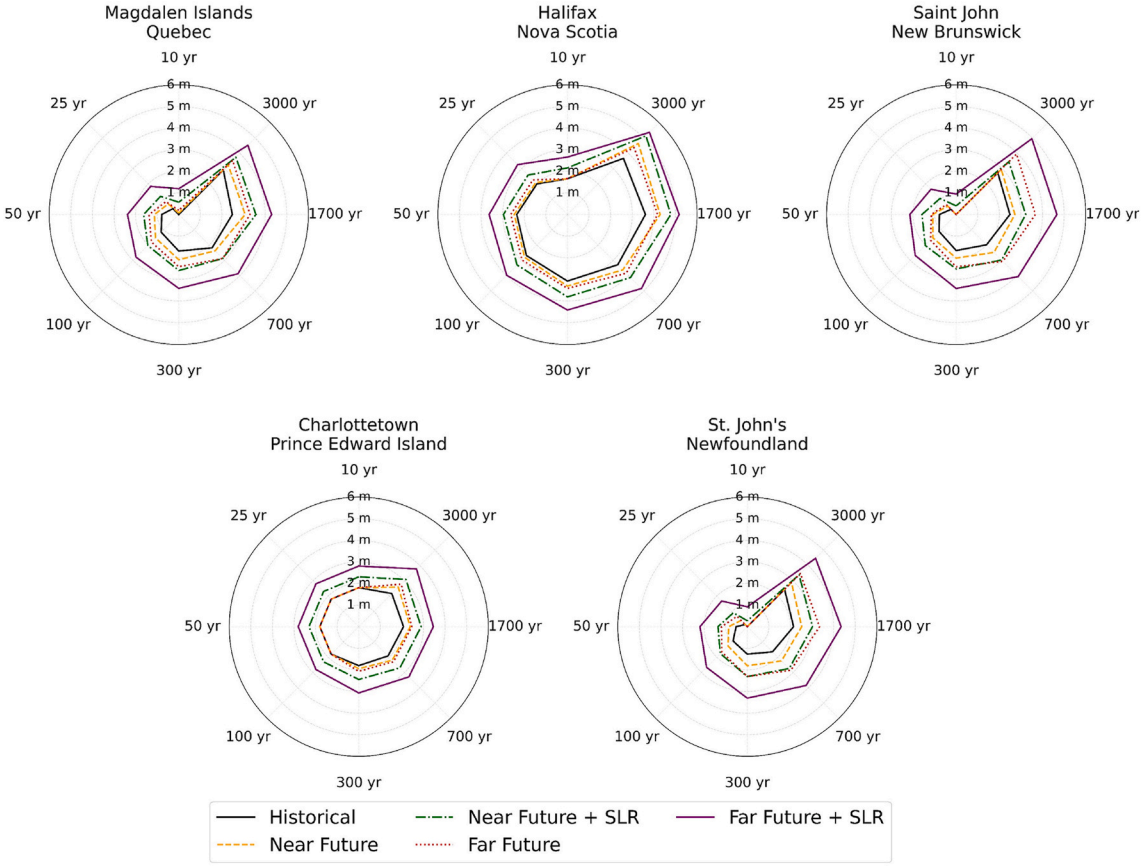

Fig. 11. Comparison of historical and projected coastal flooding return periods at selected locations, with projections driven by the EC-Earth3P-HR model.

comparatively broad-band response in wind hazard across coastal Atlantic Canada, and (ii) a more spatially concentrated flood-hazard response in low-elevation coastal zones. Within the simplified flood module used here, projected increases in coastal water-level exceedances are dominated by relative sea-level rise under SSP5-8.5, which effectively shifts baseline water levels upward between historical and future periods. Processes such as astronomical tides, wave setup/runup, and compound hydrologic contributions influence absolute water levels at specific sites, but they are not represented in the present screening framework and would require fully coupled, locally calibrated modeling for site-specific design applications. Finally, two dimensions of uncertainty are particularly relevant for adaptation planning: non-stationarity of the climate signal over time, and divergence between GCM-driven projections. The larger changes found in the far-future period relative to the near-future points to an accelerating hazard environment that favors adaptive strategies capable of being scaled over time. At the same time, the combination of decreasing encounter frequency and increasing intensity underscores that plausible futures include fewer but stronger storms, reinforcing the need for robust decision-making approaches that do not rely on a single deterministic projection.

4.2. *Methodological considerations and limitations*

The methodology employed offers several strengths, including the use of a physics-based synthetic track model to generate large statistical ensembles and the explicit assessment of non-stationarity in future TC behavior. However, several limitations and uncertainties must be acknowledged. First, the hazard simulations are restricted to TCs and do not explicitly represent baroclinic extratropical cyclones or the full extratropical transition (ET) process. This limitation is relevant for Atlantic Canada, where a substantial fraction of impactful windstorms involve post-tropical systems and/or ET dynamics (e.g., frontal development, baroclinic energy conversion, and expanded wind fields). Accordingly, the results should be interpreted as quantifying TC-related wind risk rather than the full climatology of damaging windstorms in the region. Extending synthetic downscaling and wind-field representations to better capture post-tropical structure and ET dynamics remains an important direction for future work, particularly for mid-to high-latitude coastal regions (Bloemendaal et al., 2020). Second, future projections are inherently subject to GCM-related uncertainty. Considerable divergence is observed between the two GCM-driven perturbations used here, and the analysis does not sample the full CMIP6 ensemble or alternative SSP pathways. Rather, a limited number of GCMs was selected to balance computational feasibility with the generation of long (10,000-year) synthetic catalogs for each period.

Third, the delta-change approach applied to GCM fields reduces some systematic biases but also introduces limitations. Because the method perturbs reanalysis forcing primarily through mean-state shifts, it may not fully capture changes in circulation regimes, storm-track structure, or synoptic variability that could influence steering flow and track density at higher latitudes. In this context, the North Atlantic Subtropical High (NASH, also referred to as the Azores or Bermuda High) is a semipermanent large-scale feature that exerts a strong control on the environmental steering flow of Atlantic TCs (Davis et al., 1997). Its variability also modulates the Caribbean Low-Level Jet, which influences regional cyclogenesis and low-level wind shear upstream of Atlantic Canada (Wang, 2007). Projected changes in the position or intensity of the NASH under warming could therefore alter both TC formation rates and recurvature patterns in ways that are not fully resolved by a mean-state delta perturbation approach. Reanalysis-based forcing may also carry residual biases in extreme-wind regimes, motivating cautious interpretation of local return levels and supporting the use of regional design-code benchmarks as a consistency check (Chen et al., 2024). More broadly, local extremes in synthetic cyclone datasets

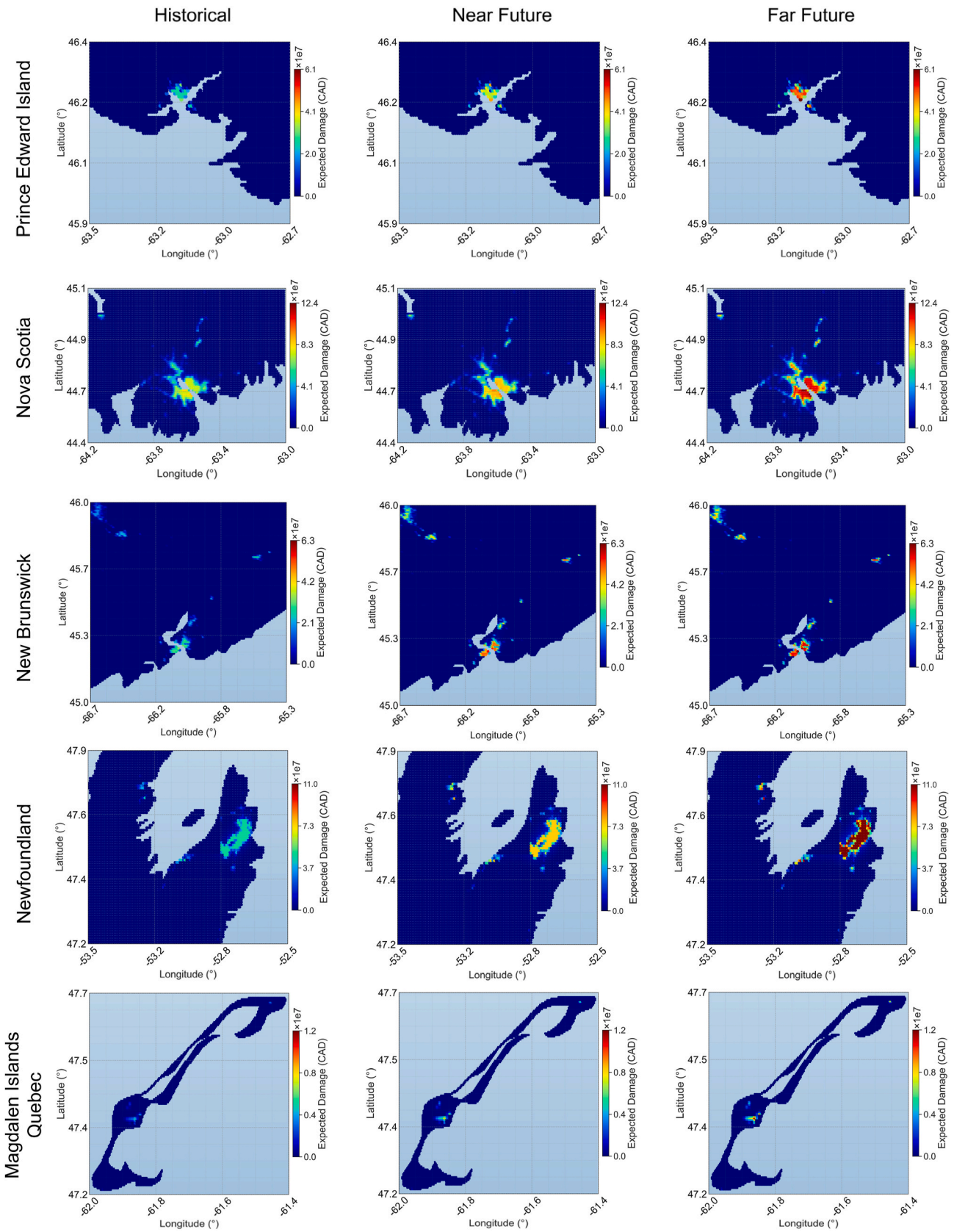

Fig. 12. Spatial distribution of Expected Damage (*ED*) from the 100-year wind hazard under historical and future scenarios (EC-Earth3P-HR).

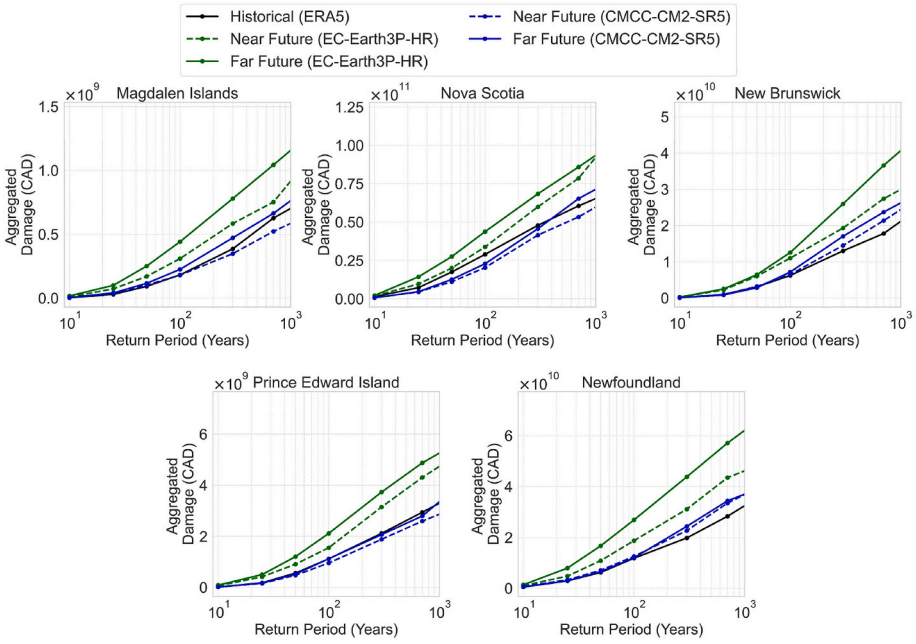

Fig. 13. Projected Aggregated Damage from wind across various return periods for selected Atlantic Canada regions.

can remain difficult to validate robustly when observational constraints are limited. These considerations emphasize that the results are scenario-conditional and that a broader multi-GCM/multi-SSP ensemble would be required to more comprehensively characterize uncertainty in future TC hazard and risk projections (Bloemendaal et al., 2020; Romero et al., 2025). Future work could test the robustness of these findings by comparing them with alternative statistical delta-based approaches applied directly to the model outputs. Fourth, the hazard models themselves introduce additional approximations. The wind field calculation relies on parametric relationships, while the bathtub flood model represents a substantial simplification of flood dynamics because it neglects hydrodynamic processes and wave action. In addition, the use of a simplified empirical relationship to estimate storm surge from wind speed is a key limitation, as the true response is highly sensitive to local bathymetry. The exclusion of astronomical tides is another simplification that could affect peak water levels (Saviz Naeini et al., 2025).

Fifth, the coastal flood hazard component is intentionally simplified and does not explicitly represent tide-surge-wave interactions or long-period oscillatory variability such as the 18.6-year lunar nodal cycle. As a result, tidal-phase modulation of peak water levels is not captured, which can be important in Atlantic Canada, particularly in high-tide-range settings such as the Bay of Fundy and other embayments (Swatridge et al., 2025). Flood estimates also inherit compounded uncertainty from the wind-to-surge parameterization, the static bathtub assumption, DEM vertical errors and datum consistency, and the exclusion of tides, waves, and precipitation-driven (pluvial and fluvial) contributions. Accordingly, the flood results are interpreted as relative, screening-level indicators of how surge potential and baseline sea-level rise may shift inundation susceptibility between time periods under consistent assumptions, rather than as absolute event-specific flood levels for design. More detailed assessments would require coupled hydrodynamic, wave, and tide modeling with local calibration, and extending such models to large synthetic-event catalogs remains an important direction for future work. Sixth, simulated wind footprints depend on the empirical specification of R_{max}, which controls the radial scale of the storm wind field. A targeted sensitivity perturbation of $\pm 10\%$ in R_{max} suggests modest effects on aggregate hazard statistics (approximately a 1% change in domain-mean wind intensity), while impacts can be larger locally near the storm core and for individual events. Systematic bias in R_{max} could therefore influence coastal wind exceedances and wind-driven surge estimates, highlighting the need for future work that addresses broader parametric uncertainty and improves representation of post-tropical structure at higher latitudes.

Finally, the risk components (exposure and vulnerability) are a major source of uncertainty. A key assumption in this study is that while the hazard evolves with climate change, the socio-economic landscape remains static. Future changes in exposure (e.g., population growth, new coastal development) and vulnerability (e.g., improved building codes or age-related degradation of infrastructure) are not considered. Moreover, nighttime light intensity scaled by provincial GDP per capita is used to construct a regional-scale proxy for direct socio-economic exposure where detailed asset inventories are unavailable. This proxy does not represent critical infrastructure, network connectivity, or systemic economic dependencies in low-population corridors (e.g., transportation lifelines), and it does not distinguish between insured and uninsured assets or sector-specific vulnerabilities. Consequently, absolute loss estimates are skewed toward densely populated and economically active areas and should not be interpreted as indicators of social vulnerability, equity, or broader indirect and cascading economic impacts. In addition, the vulnerability function adapted from Emanuel's work requires assumptions regarding its applicability to building archetypes in Atlantic Canada. In this context, the wind-proxy approach provides a useful baseline for regional risk evaluation, but it does not capture the full spectrum of coastal damages, particularly from flooding. Reliable quantitative flood-loss estimation would require building-level exposure inventories and regionally calibrated flood depth–damage functions (e.g., HAZUS-type curves) combined with high-resolution hazard data. Lastly, potential interactions between hazards (e.g., wind damage increasing vulnerability to flooding) and rainfall-driven compound flooding processes are not considered.

4.3. Implications for adaptation and research priorities

Projected increases in wind-driven loss potential and coastal-flood hazard, together with clear non-stationarity, call for adaptation that looks beyond historical baselines toward forward-looking planning. Land-use policy and infrastructure design should incorporate elevated future wind loads and flood levels, including sea-level rise, across relevant design lifetimes. Risk hotspot maps can guide zoning by limiting

new development in the most exposed areas and by elevating construction standards in zones with increasing risk. Disaster risk reduction should be multi-hazard, combining improved early warning, evacuation and sheltering strategies that reflect the different spatial footprints of wind and flooding. Community programs, emergency planning, and asset management should be informed by the projected geographic shifts in exposure and loss potential. Integrated and adaptive pathways are essential. Planning should address wind and flood jointly, recognizing that the dominant driver varies by location and may evolve over time. Given uncertainty and potential acceleration, adaptation plans should be flexible and iterative, with predefined monitoring indicators and trigger points for updating standards, investments, and land-use decisions as new information becomes available.

Several research priorities follow from these findings. First, hazard characterization would benefit from higher-resolution climate inputs, improved downscaling and bias-correction methods, and for coastal flooding, replacement of the bathtub approach with hydrodynamic modeling that resolves timing, velocities, and wave effects, as well as the use of gridded, spatially varying relative SLR fields (or tide-gauge-specific SLR values) that incorporate local vertical land motion (subsidence/uplift). Second, exposure and vulnerability components require refinement through region-specific vulnerability functions for Atlantic Canada building archetypes, calibrated with local claims and inspection data, and through a consistent exposure database useable for both wind and flood analyses. Third, the scope of risk assessment should expand to compound events, such as storm surge coincident with heavy rainfall, and to dynamic interactions where wind damage alters subsequent flood vulnerability. Embedding specific adaptation measures, including seawalls, building elevation, critical-asset hardening, and zoning changes, directly within the risk-modeling workflow would enable comparative effectiveness analysis. Fourth, future work should incorporate changes in exposure and vulnerability over time, reflecting urban growth, asset value escalation, demographic shifts, infrastructure aging, retrofit and code adoption rates, and managed retreat. This can be implemented through inventory-evolution modules linked to socioeconomic pathways and time-stamped fragility functions that update with materials, design standards, and adaptation uptake. Finally, broader multi-model ensembles across GCMs and SSPs, coupled with explicit uncertainty quantification, can provide more robust decision support for design codes, insurance pricing, and public investment.

5. Conclusion

This study presented a quantitative assessment of evolving tropical cyclone (TC) threats in Atlantic Canada, characterizing future changes in both wind and coastal flood hazards and estimating the resulting total TC risk using a wind-proxy methodology. The findings indicate a complex and accelerating threat profile with projected changes that are GCM-dependent and spatially heterogeneous. Wind hazard increases are generally widespread under EC-Earth3P-HR, whereas CMCC-CM2-SR5 yields a more mixed spatial response with localized increases and decreases. Across scenarios, results are consistent with a plausible future characterized by fewer storm encounters but higher storm intensity, leading to increased wind hazard and higher wind-proxy losses in many coastal areas, including parts of Nova Scotia and Newfoundland and Labrador. For coastal flooding, relative sea-level rise is the dominant driver of increasing hazard within the screening-level surge + SLR framework, strongly amplifying the effects of changes in storm characteristics; absolute water levels would additionally be modulated by tides, waves, and river discharge, which are not represented in this assessment. The study highlights significant uncertainty in the magnitude of future risk due to divergent outcomes from the climate models. Most importantly, the spatial analysis reveals that the highest absolute wind-proxy losses are concentrated in urbanized coastal communities, where dense exposure intersects with intensifying wind hazard. These areas therefore face the greatest escalation in absolute economic losses across the projected scenarios. While a dedicated flood risk assessment (hazard coupled with exposure and vulnerability) was beyond the scope of this work, the flood results provide useful screening-level evidence of where inundation susceptibility may increase under consistent assumptions. Accordingly, these flood hazard maps are intended to indicate the direction and relative magnitude of plausible changes in inundation potential, rather than absolute event-specific flood levels for design. Using a wind-proxy approach, consistent with standard practice in large-scale risk assessment, provides a practical baseline estimate of escalating economic impacts. Overall, this work delivers a quantitative, forward-looking picture of Atlantic Canada's evolving TC risk environment and supports the development of proactive, spatially targeted adaptation strategies that remain robust under non-stationary and multi-hazard conditions.

CRediT authorship contribution statement

Saeed Saviz Naeini: Writing – review & editing, Writing – original draft, Visualization, Validation, Software, Methodology, Investigation, Formal analysis, Data curation, Conceptualization. **Reda Snaiki:** Writing – review & editing, Writing – original draft, Supervision, Resources, Project administration, Methodology, Investigation, Funding acquisition, Formal analysis, Conceptualization. **Alejandro Di Luca:** Writing – review & editing, Writing – original draft, Supervision, Methodology, Investigation, Formal analysis, Conceptualization.

Declaration of competing interest

The authors declare that they have no known competing financial interests or personal relationships that could have appeared to influence the work reported in this paper.

Acknowledgements

This work was supported by the Natural Sciences and Engineering Research Council of Canada (NSERC) [grant number CRSNG RGPIN 2022-03492] and AdapT – Institut de recherche sur les infrastructures résilientes et circulaires.

Data availability

Data will be made available on request.

References

Almeida, L.S., Goerlandt, F., Pelot, R., 2019. Effects of major hurricanes in Atlantic Canada from 2003 to 2018. In: Risk Analysis Based on Data and Crisis Response Beyond Knowledge. CRC Press.

Aziz, E., 2021. Key lessons from hurricane dorian: the benefits of a flexible top-down storm response. J. Bus. Continuity Emerg. Plan. 15 (2), 158–170.

Aznar-Siguan, G., Bresch, D.N., 2019. CLIMADA v1: a global weather and climate risk assessment platform. Geosci. Model Dev. (GMD) 12 (7), 3085–3097.

Balaguru, K., Xu, W., Chang, C.-C., Leung, L.R., Judi, D.R., Hagos, S.M., Wehner, M.F., Kossin, J.P., Ting, M., 2023. Increased U.S. coastal hurricane risk under climate change. Sci. Adv. 9 (14), eadf0259.

Bloemendaal, N., Haigh, I.D., de Moel, H., Muis, S., Haarsma, R.J., Aerts, J.C.J.H., 2020. Generation of a global synthetic tropical cyclone hazard dataset using STORM. Sci. Data 7 (1), 40.

Buttle, J.M., Allen, D.M., Caissie, D., Davison, B., Hayashi, M., Peters, D.L., Pomeroy, J. W., Simonovic, S., St-Hilaire, A., Whitfield, P.H., 2016. Flood processes in Canada: regional and special aspects. Can. Water Resour. J./Revue Canadienne Des Ressources Hydriques 41 (1–2), 7–30.

Canada, N.R., 2019. High Resolution Digital Elevation Model (HRDEM)–canElevation Series–Product Specifications.

Carney, M., Kantz, H., Nicol, M., 2022. Hurricane Simulation and Nonstationary Extremal Analysis for a Changing Climate.

Chen, T.-C., Collet, F., Di Luca, A., 2024. Evaluation of ERA5 precipitation and 10-m wind speed associated with extratropical cyclones using station data over North America. Int. J. Climatol. 44 (3), 729–747.

Chouinard, O., Plante, S., Weissenberger, S., Noblet, M., Guillemot, J., 2017. The participative action research approach to climate change adaptation in Atlantic Canadian coastal communities. In: Leal Filho, W., Keenan, J.M. (Eds.), Climate

Change Adaptation in North America: Fostering Resilience and the Regional Capacity to Adapt. Springer International Publishing, pp. 67–87.
Cousineau, J., Murphy, E., 2022. Numerical investigation of climate change effects on storm surges and extreme waves on canada's Pacific Coast. Atmosphere 13 (2), 311.
Davis, R.E., Hayden, B.P., Gay, D.A., Phillips, W.L., Jones, G.V., 1997. The North Atlantic Subtropical Anticyclone.
Didier, D., Baudry, J., Bernatchez, P., Dumont, D., Sadegh, M., Bismuth, E., Bandet, M., Dugas, S., Sévigny, C., 2019. Multihazard simulation for coastal flood mapping: bathtub versus numerical modelling in an open estuary, eastern Canada. J. Flood Risk Manag. 12 (S1), e12505.
Do, C., Kuleshov, Y., 2023. Multi-hazard tropical cyclone risk assessment for Australia. Remote Sens 15 (3), 795.
Eberenz, S., Lüthi, S., Bresch, D.N., 2021. Regional tropical cyclone impact functions for globally consistent risk assessments. Nat. Hazards Earth Syst. Sci. 21 (1), 393–415.
Emanuel, K., 2005. Increasing destructiveness of tropical cyclones over the past 30 years. Nature 436 (7051), 686–688.
Emanuel, K., 2011. Global Warming Effects on U.S. Hurricane Damage.
Emanuel, K., 2017. A fast intensity simulator for tropical cyclone risk analysis. Nat. Hazards 88 (2), 779–796.
Emanuel, K., 2022. Tropical Cyclone Seeds, Transition Probabilities, and Genesis.
Emanuel, K., Ravela, S., Vivant, E., Risi, C., 2006. A Statistical Deterministic Approach to Hurricane Risk Assessment.
Forzieri, G., Feyen, L., Russo, S., Vousdoukas, M., Alfieri, L., Outten, S., Migliavacca, M., Bianchi, A., Rojas, R., Cid, A., 2016. Multi-hazard assessment in Europe under climate change. Clim. Change 137 (1), 105–119.
Garin, A., Pausata, F.S.R., Boudreault, M., Ingrosso, R., 2024. The Impacts of Climate Change on tropical-to-extratropical Transitions in the North-Atlantic Basin *Egusphere*, pp. 1–24.
Gori, A., Lin, N., Xi, D., Emanuel, K., 2022. Tropical cyclone climatology change greatly exacerbates US extreme rainfall–surge hazard. Nat. Clim. Change 12 (2), 171–178.
Hall, A., Rahimi, S., Norris, J., Ban, N., Siler, N., Leung, L.R., Ullrich, P., Reed, K.A., Prein, A.F., Qian, Y., 2024. An evaluation of dynamical downscaling methods used to project regional climate change. J. Geophys. Res. Atmos. 129 (24) e2023JD040591.
Harper, B., Kepert, J., Ginger, J., 2010. Guidelines for Converting Between Various Wind Averaging Periods in Tropical Cyclone Conditions.
Hart, R.E., Evans, J.L., 2001. A Climatology of the Extratropical Transition of Atlantic Tropical Cyclones.
Hersbach, H., Bell, B., Berrisford, P., Hirahara, S., Horányi, A., Muñoz-Sabater, J., Nicolas, J., Peubey, C., Radu, R., Schepers, D., Simmons, A., Soci, C., Abdalla, S., Abellan, X., Balsamo, G., Bechtold, P., Biavati, G., Bidlot, J., Bonavita, M., et al., 2020. The ERA5 global reanalysis. Q. J. R. Meteorol. Soc. 146 (730), 1999–2049.
Hillier, J.K., Matthews, T., Wilby, R.L., Murphy, C., 2020. Multi-hazard dependencies can increase or decrease risk. Nat. Clim. Change 10 (7), 595–598.
Holland, G., 1980. An analytic model of the wind and pressure profiles in hurricanes. Mon. Weather Rev. 108, 1212–1218.
Jiang, J., Perrie, W., 2008. Climate change effects on north Atlantic cyclones. J. Geophys. Res. Atmos. 113 (D9).
Jung, C., Lackmann, G.M., 2023. Changes in tropical cyclones undergoing extratropical transition in a warming climate: quasi-idealized numerical experiments of north Atlantic landfalling events. Geophys. Res. Lett. 50 (8) e2022GL101963.
Kameshwar, S., Padgett, J.E., 2014. Multi-hazard risk assessment of highway bridges subjected to earthquake and hurricane hazards. Engineering Structures, Performance Based Engineering: Current Advances and Applications 78, 154–166.
Knutson, T.R., Sirutis, J.J., Garner, S.T., Vecchi, G.A., Held, I.M., 2008. Simulated reduction in Atlantic hurricane frequency under twenty-first-century warming conditions. Nat. Geosci. 1 (6), 359–364.
Knutson, T.R., Sirutis, J.J., Zhao, M., Tuleya, R.E., Bender, M., Vecchi, G.A., Villarini, G., Chavas, D., 2015. Global Projections of Intense Tropical Cyclone Activity for the Late Twenty-First Century from Dynamical Downscaling of CMIP5/RCP4.5 Scenarios.
Kossin, J.P., 2018. A global slowdown of tropical-cyclone translation speed. Nature 558 (7708), 104–107.
Lee, H., Calvin, K., Dasgupta, D., Krinner, G., Mukherji, A., Thorne, P., Trisos, C., Romero, J., Aldunce, P., Barret, K., Blanco, G., Cheung, W.W.L., Connors, S.L., Denton, F., Diongue-Niang, A., Dodman, D., Garschagen, M., Geden, O., Hayward, B., et al., 2023. IPCC, 2023: climate change 2023: Synthesis report, summary for policymakers. In: Lee, H., Romero, J. (Eds.), Contribution of Working Groups I, II and III to the Sixth Assessment Report of the Intergovernmental Panel on Climate Change [Core Writing Team. Intergovernmental Panel on Climate Change (IPCC), *IPCC, Geneva, Switzerland. [Mo*nograph].
Li, S.H., 2023. Effect of nonstationary extreme wind speeds and ground snow loads on the structural reliability in a future Canadian changing climate. Struct. Saf. 101, 102296.
Li, S.H., Irwin, P., Lounis, Z., Attar, A., Dale, J., Gibbons, M., Beaulieu, S., 2022. Effects of nonstationarity of extreme wind speeds and ground snow loads in a future Canadian changing climate. Nat. Hazards Rev. 23 (4), 04022022.
Lin, N., Chavas, D., 2012. On hurricane parametric wind and applications in storm surge modeling. J. Geophys. Res. Atmos. 117 (D9). https://doi.org/10.1029/2011JD017126.
Lin, H., Mo, R., Vitart, F., Stan, C., 2019. Eastern Canada flooding 2017 and its subseasonal predictions. Atmos.-Ocean 57 (3), 195–207.
Lin, I.-I., Camargo, S.J., Lien, C.-C., Shi, C.-A., Kossin, J.P., 2023a. Poleward migration as global warming's possible self-regulator to restrain future Western north Pacific tropical Cyclone's intensification. npj Clim. Atmos. Sci. 6 (1), 34.
Lin, J., Rousseau-Rizzi, R., Lee, C.-Y., Sobel, A., 2023b. An open-source, physics-based, tropical cyclone downscaling model with intensity-dependent steering. J. Adv. Model. Earth Syst. 15 (11) e2023MS003686.
Liu, A., 2024. Integrated Multi-Hazard and Vulnerability Modelling for Flood Risk Assessment in the US Gulf Coast [Masters, Department of Risk and Disaster Reduction]. In: Masters Thesis, Department of Risk and Disaster Reduction.
Makkonen, L., 2006. Plotting Positions in Extreme Value Analysis.
Manuel, P., Rapaport, E., Keefe, J., Krawchenko, T., 2015. Coastal climate change and aging communities in Atlantic Canada: a methodological overview of community asset and social vulnerability mapping. Canadian Geographies/Géographies Canadiennes 59 (4), 433–446.
Masson, A., 2014. The extratropical transition of hurricane igor and the impacts on Newfoundland. Nat. Hazards 72 (2), 617–632.
Mendez-Tejeda, R., Hernández-Ayala, J., 2023. Links between climate change and hurricanes in the north Atlantic. PLOS Climate 2, e0000186.
Meng, Y., Matsui, M., Hibi, K., 1995. An analytical model for simulation of the wind field in a typhoon boundary layer. J. Wind Eng. Ind. Aerod. 56 (2), 291–310.
Naeini, S.S., Snaiki, R., 2024. A novel hybrid machine learning model for rapid assessment of wave and storm surge responses over an extended coastal region. Coast. Eng. 190, 104503.
Nofal, O.M., van de Lindt, J.W., Do, T.Q., Yan, G., Hamideh, S., Cox, D.T., Dietrich, J.C., 2021. Methodology for regional multihazard hurricane damage and risk assessment. J. Struct. Eng. 147 (11), 04021185.
Nofal, O.M., Amini, K., Padgett, J.E., van de Lindt, J.W., Rosenheim, N., Darestani, Y.M., Enderami, A., Sutley, E.J., Hamideh, S., Duenas-Osorio, L., 2023. Multi-hazard socio-physical resilience assessment of hurricane-induced hazards on coastal communities. Resilient Cities and Structures, Integrated Modeling of Cities to Improve Natural Hazards Resilience 2 (2), 67–81.
Pang, T., Shah, M.A.R., Dau, Q.V., Wang, X., 2024. Assessing the social risks of flooding for coastal societies: a case study for Prince Edward Island, Canada. Environ. Res. Commun. 6 (7), 075027.
Plante, M., Son, S.-W., Atallah, E., Gyakum, J., Grise, K., 2015. Extratropical cyclone climatology across eastern Canada. Int. J. Climatol. 35 (10), 2759–2776.
Poulter, B., Halpin, P.N., 2008. Raster modelling of coastal flooding from sea-level rise. Int. J. Geogr. Inf. Sci. 22 (2), 167–182.
Prein, A.F., Liu, C., Ikeda, K., Trier, S.B., Rasmussen, R.M., Holland, G.J., Clark, M.P., 2017. Increased rainfall volume from future convective storms in the US. Nat. Clim. Change 7 (12), 880–884.
Provan, M., Ferguson, S., Murphy, E., 2022. Storm surge contributions to flood hazards on Canada's Atlantic Coast. J. Flood Risk Manag. 15 (3), e12800.
Rana, A., Zhu, Q., Detken, A., Whalley, K., Castet, C., 2022. Strengthening climate-resilient development and transformation in Viet Nam. Clim. Change 170 (1), 4.
Rasmussen, R., Liu, C., Ikeda, K., Gochis, D., Yates, D., Chen, F., Tewari, M., Barlage, M., Dudhia, J., Yu, W., Miller, K., Arsenault, K., Grubišić, V., Thompson, G., Gutmann, E., 2011. High-Resolution Coupled Climate Runoff Simulations of Seasonal Snowfall over Colorado: a Process Study of Current and Warmer Climate.
Reed, K.A., Wehner, M.F., Zarzycki, C.M., 2022. Attribution of 2020 hurricane season extreme rainfall to human-induced climate change. Nat. Commun. 13 (1), 1905.
Román, M.O., Wang, Z., Sun, Q., Kalb, V., Miller, S.D., Molthan, A., Schultz, L., Bell, J., Stokes, E.C., Pandey, B., Seto, K.C., Hall, D., Oda, T., Wolfe, R.E., Lin, G., Golpayegani, N., Devadiga, S., Davidson, C., Sarkar, S., et al., 2018. NASA's black marble nighttime lights product suite. Rem. Sens. Environ. 210, 113–143.
Romero, D., Appendini, C.M., Emanuel, K., Lee, C.-Y., Nederhoff, K., Bloemendaal, N., Ruiz-Salcines, P., Vigh, J., Domínguez, C., 2025. Assessment of synthetic tropical cyclones in the north Atlantic basin. Atmos. Res., 108404
Ryan, B., Bristow, D.N., 2024. Risk assessment framework of adapting coastal infrastructure to climate change. AIP Conf. Proc. 3215 (1), 020009.
Sahoo, B., Bhaskaran, P.K., 2018. Multi-hazard risk assessment of coastal vulnerability from tropical cyclones – a GIS based approach for the Odisha coast. J. Environ. Manag. 206, 1166–1178.
Salarieh, B., Ugwu, I.A., Salman, A.M., 2023. Impact of changes in sea surface temperature due to climate change on hurricane wind and storm surge hazards across US Atlantic and gulf coast regions. SN Appl. Sci. 5 (8), 205.
Saviz Naeini, S., Snaiki, R., Wu, T., 2025. Advancing spatio-temporal storm surge prediction with hierarchical deep neural networks. Nat. Hazards.
Schär, C., Frei, C., Lüthi, D., Davies, H.C., 1996. Surrogate climate-change scenarios for regional climate models. Geophys. Res. Lett. 23 (6), 669–672.
Seneviratne, S.I., Zhang, X., Adnan, M., Badi, W., Dereczynski, C., Di Luca, A., Ghosh, S., Iskandar, I., Kossin, J., Lewis, S., Otto, F., Pinto, I., Satoh, M., Vicente-Serrano, S.M., Wehner, M., Zhou, B., 2021. Weather and climate extreme events in a changing climate. In: MassonDelmotte, V., Zhai, P., Pirani, A., Connors, S.L., Péan, C., Berger, S., Caud, N., Chen, Y., Goldfarb, L., Gomis, M.I., Huang, M., Leitzell, K., Lonnoy, E., Matthews, J.B.R., Maycock, T.K., Waterfield, T., Yelekçi, O., Yu, R., Zh, B. (Eds.), Climate Change 2021: the Physical Science Basis. Contribution of Working Group I to the Sixth Assessment Report of the Intergovernmental Panel on Climate Change, pp. 1513–1766.
Shepard, C.C., Agostini, V.N., Gilmer, B., Allen, T., Stone, J., Brooks, W., Beck, M.W., 2012. Assessing future risk: quantifying the effects of sea level rise on storm surge risk for the southern shores of Long Island, New York. Nat. Hazards 60 (2), 727–745.
Snaiki, R., Parida, S.S., 2023. A data-driven physics-informed stochastic framework for hurricane-induced risk estimation of transmission tower-line systems under a changing climate. Eng. Struct. 280, 115673.
Snaiki, R., Wu, T., 2017. Modeling tropical cyclone boundary layer: height-resolving pressure and wind fields. J. Wind Eng. Ind. Aerod. 170, 18–27.
Snaiki, R., Wu, T., 2025. A Novel Dynamic Bias-Correction Framework for Hurricane Risk Assessment Under Climate Change. Arxiv Preprint arXiv:2505.00832.
Stalhandske, Z., Steinmann, C.B., Meiler, S., Sauer, I.J., Vogt, T., Bresch, D.N., Kropf, C. M., 2024. Global multi-hazard risk assessment in a changing climate. Sci. Rep. 14 (1), 5875.

Straub, A.M., 2024. Post-tropical cyclone fiona and Atlantic Canada: media framing of hazard risk in the anthropocene. Disasters 48 (4), e12641.
Studholme, J., Fedorov, A.V., Gulev, S.K., Emanuel, K., Hodges, K., 2022. Poleward expansion of tropical cyclone latitudes in warming climates. Nat. Geosci. 15 (1), 14–28.
Swatridge, L.L., Mulligan, R.P., Boegman, L., Shan, S., Murphy, E., 2025. Insight on the coastal response to combined tides, storm surges, and surface waves in a macrotidal bay from real-time predictions. J. Geophys. Res., Oceans 130 (9) e2024JC022076.
Taylor, A.R., Dracup, E., MacLean, D.A., Boulanger, Y., Endicott, S., 2019. Forest structure more important than topography in determining windthrow during hurricane juan in Canada's acadian forest. For. Ecol. Manag. 434, 255–263.
Thompson, K.R., Bernier, N.B., Chan, P., 2009. Extreme sea levels, coastal flooding and climate change with a focus on Atlantic Canada. Nat. Hazards 51 (1), 139–150.
Tilloy, A., Malamud, B.D., Winter, H., Joly-Laugel, A., 2019. A review of quantification methodologies for multi-hazard interrelationships. Earth Sci. Rev. 196, 102881.
Trepanier, J.C., 2020. North Atlantic hurricane winds in warmer than normal seas. Atmosphere 11 (3), 293.
Tu, S., Chan, J.C.L., Xu, J., Zhong, Q., Zhou, W., Zhang, Y., 2022. Increase in tropical cyclone rain rate with translation speed. Nat. Commun. 13 (1), 7325.
Vasseur, L., Thornbush, M., Plante, S., 2017. Climatic and environmental changes affecting communities in Atlantic Canada. Sustainability 9 (8), 1293.
Vasseur, L., Thornbush, M.J., Plante, S., 2022. Engaging communities in adaptation to climate change by understanding the dimensions of social capital in Atlantic Canada. Sustainability 14 (9), 5250.
Walsh, K.J.E., McBride, J.L., Klotzbach, P.J., Balachandran, S., Camargo, S.J., Holland, G., Knutson, T.R., Kossin, J.P., Lee, T., Sobel, A., Sugi, M., 2016. Tropical cyclones and climate change. WIREs Clim. Change 7 (1), 65–89.
Wang, C., 2007. Variability of the Caribbean low-level jet and its relations to climate. Clim. Dyn. 29 (4), 411–422.
Ward, P.J., Daniell, J., Duncan, M., Dunne, A., Hananel, C., Hochrainer-Stigler, S., Tijssen, A., Torresan, S., Ciurean, R., Gill, J.C., Sillmann, J., Couasnon, A., Koks, E., Padrón-Fumero, N., Tatman, S., Tronstad Lund, M., Adesiyun, A., Aerts, J.C.J.H., Alabaster, A., et al., 2022. Invited perspectives: a research agenda towards disaster risk management pathways in multi-(hazard-)risk assessment. Nat. Hazards Earth Syst. Sci. 22 (4), 1487–1497.
Weibull, W., 1939. A Statistical Theory of Strength of Materials. *IVB-handl*.
Willison, J., Robinson, W.A., Lackmann, G.M., 2015. North Atlantic Storm-Track Sensitivity to Warming Increases with Model Resolution.
Xu, L., 2010. A simple coastline storm surge model based on pre-run SLOSH outputs. 29th Conference on Hurricanes and Tropical Meteorology (10-14 May 2010).
Zadra, A., McTaggart-Cowan, R., Vaillancourt, P.A., Roch, M., Bélair, S., Leduc, A.-M., 2014. Evaluation of Tropical Cyclones in the Canadian Global Modeling System: Sensitivity to Moist Process Parameterization.